Disproportionate investment in Spiralin B production limits in-host growth and favors the vertical transmission of *Spiroplasma* insect endosymbionts

Florent Masson[a,1,2,3], Samuel Rommelaere[a,1], Fanny Schüpfer[a], Jean-Philippe Boquete[a], and Bruno Lemaitre[a,3]

Insects frequently harbor endosymbionts, which are bacteria housed within host tissues. These associations are stably maintained over evolutionary timescales through vertical transmission of endosymbionts from host mothers to their offspring. Some endosymbionts manipulate host reproduction to facilitate spread within natural populations. Consequently, such infections have major impacts on insect physiology and evolution. However, technical hurdles have limited our understanding of the molecular mechanisms underlying such insect–endosymbiont interactions. Here, we investigate the nutritional interactions between endosymbiotic partners using the tractable insect *Drosophila melanogaster* and its natural endosymbiont *Spiroplasma poulsonii*. Using a combination of functional assays, metabolomics, and proteomics, we show that the abundance and amino acid composition of a single *Spiroplasma* membrane lectin, Spiralin B (SpiB), dictates the amino acid requirements of the endosymbiont and determines its proliferation within host tissues. Ectopically increasing SpiB levels in host tissues disrupts localization of endosymbionts in the fly egg chambers and decreases vertical transmission. We find that SpiB is likely to be required by the endosymbiont to enter host oocytes, which may explain the massive investment of *S. poulsonii* in SpiB synthesis. SpiB both permits vertical transmission of the symbiont and limits its growth in nutrient-limiting conditions for the host; therefore, a single protein plays a pivotal role in ensuring durability of the interaction in a variable environment.

endosymbiosis | symbiosis | *Spiroplasma* | vertical transmission | Spiralin

Insects frequently harbor endosymbionts, which are microbial symbionts housed within their tissues. Endosymbiotic interactions have major impacts on insect evolution as endosymbionts affect host development, physiology, and reproduction (1–3). The most widespread insect endosymbionts in nature are reproductive manipulators (4, 5). These encompass bacterial species from diverse taxa that infect the host germ line and are transmitted vertically. They alter host reproduction through four distinct mechanisms: cytoplasmic incompatibility, male-killing, feminization, and induction of parthenogenesis. These mechanisms create an evolutionary drive that favors infected hosts and participates in propagating the endosymbiotic infection through host populations (6, 7). Beyond their effects on host reproduction, reproductive manipulators are often associated with beneficial phenotypes for the host. For example, *Wolbachia*, a genus of reproductive manipulator detected in 20 to 40% of insect species including pests and disease vectors (4, 5), confers some of its hosts with protection against viruses (8, 9). This feature makes artificial transfers of *Wolbachia* across species a biotechnological tool to fight the spread of arboviruses in vector populations (10). The emergence of field applications has stimulated remarkable progress in understanding the biology of reproductive manipulators. However, the molecular mechanisms underlying symbiont interactions with their hosts remain largely elusive. This knowledge gap is largely due to technical hurdles inherent to bacteria that are not culturable or genetically modifiable (3).

The genus *Spiroplasma* is a valuable model to answer these questions. This genus belongs to the Mollicutes class, which encompasses bacteria lacking a cell wall that live in obligate associations with eukaryotic hosts (11). It includes diverse species ranging from plant and insect pathogens to vertically transmitted endosymbionts. One species, *Spiroplasma poulsonii* Melanogaster Sex-Ratio Organism, hereafter simply MSRO, naturally infects the fruit fly *Drosophila melanogaster* (12), which gives access to powerful genetic tools on the host side to dissect the molecular determinants of the interaction. MSRO lives extracellularly in the fly hemolymph. It is vertically inherited by infecting the female germ line during oogenesis: The bacteria cross the epithelium between the tricellular junctions of follicular cells of stage 10 egg chambers and are endocytosed by the oocyte during vitellogenesis (13, 14).

Significance

Most insects harbor bacterial endosymbionts within their tissues, which have major impacts on their physiology, ecology, and evolution. We investigate mechanisms that regulate such interaction between the fly *Drosophila* and its natural bacterial endosymbiont *Spiroplasma poulsonii* Melanogaster Sex-Ratio Organism (MSRO). MSRO grows in the fly hemolymph and is vertically transmitted across generations. We show that Spiralin B has major impacts on these two key features: while being involved in vertical transmission, its massive production monopolizes essential amino acids and impacts bacterial growth in nutrient-limited conditions. Our work illustrates that a single bacterial protein can couple key aspects of an endosymbiont lifestyle (its ability to proliferate in host tissues and to be vertically transmitted), thus maintaining the interaction over evolutionary timescales.
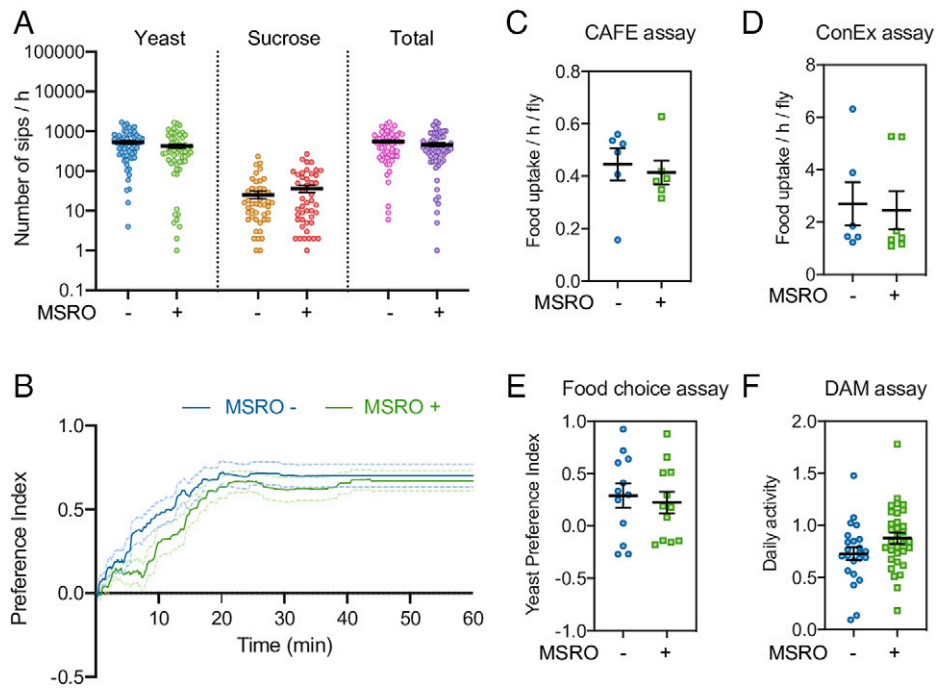
[1]F.M. and S.R. contributed equally to this work.

[2]Present address: School of Biological Sciences, University of Bristol, Bristol, BS8 1TQ, United Kingdom.

[3]To whom correspondence may be addressed. Email: florent.masson@bristol.ac.uk or bruno.lemaitre@epfl.ch.

Fig. 1. *Drosophila* feeding behavior is unchanged upon MSRO infection. (*A*) Number of FlyPad-recorded sips from uninfected (MSRO −) and MSRO-infected (MSRO +) flies given a choice to feed for 1 h on 10% yeast or 20 mM sucrose. Each dot represents a single fly, and bars represent the mean ± SEM. (*B*) FlyPad-computed cumulative preference index over 1 h. Positive values indicate a preference toward yeast over sucrose. Full lines indicate the mean and dotted lines the 95% confidence interval calculated from 62 uninfected (MSRO −) flies and 60 MSRO-infected (MSRO +) flies. (*C*) The CAFE assay quantifies the uptake of a sucrose solution (liquid food). (*D*) The ConEx assay quantifies the consumption of solid, complete food (cornmeal-agar). (*E*) The food choice assay assesses the propensity of flies to forage a sugar-rich (glucose) or a protein-rich (yeast-based) diet. (*C–E*) Each dot represents a replicate of five flies, and bars represent the mean ± SEM. (*F*) The DAM assays the locomotor activity of the flies. Each dot represents a single fly, and bars represent the mean ± SEM. Data in *A* and *C–F* were analyzed by Mann–Whitney *U* tests ($P > 0.05$).

In the hemolymph, MSRO titer increases steadily with fly aging (15). The infection has no significant consequences in young flies while it becomes deleterious in older ones, which display neurodegenerative phenotypes and have a reduced life span compared to uninfected controls (15). Deleterious phenotypes are thought to be a direct consequence of the titer increase, which becomes progressively unbearable for the fly. However, the durability of the interaction over evolutionary times relies on host fertility, both for the host itself and for the endosymbiont, which relies on vertical transmission to spread. It is therefore expected that mechanisms that keep MSRO titer in check in young, fertile flies have been selected during symbiont evolution. The availability of circulating diacylglycerides (DAGs) is one such mechanism, as lower DAG levels in the fly hemolymph impair bacterial growth (15). Similarly, the availability of Fe^{2+} ions complexed with the host iron transporter Tsf1 is a key requirement for normal MSRO proliferation (16). These two examples highlight host nutrition as a key factor regulating MSRO titer.

Here, we further investigated how host metabolic status impacts MSRO titer in young flies, with a particular focus on dietary amino acids. We found that removing any one of five key essential amino acids (EAAs) from the host diet was sufficient to block MSRO growth, while all other depletions had little to no effect. Using a combination of metabolomics and proteomics, we show that a single bacterial membrane protein with uniquely biased sequence composition and abundance, Spiralin B (SpiB), drives this peculiar nutritional requirement. Last, we leveraged *Drosophila* genetics to demonstrate that SpiB may participate in MSRO vertical transmission. Collectively, our results uncover a mechanism where MSRO massively invests specific EAAs into SpiB production, which affects both vertical transmission and in-host proliferation.

Results

1. MSRO Does Not Alter *Drosophila* Feeding Behavior. MSRO lives in *Drosophila* hemolymph, where it feeds on circulating nutrients (15). Therefore, bacterial growth is expected to cause nutritional deprivation of the host and trigger a compensatory increase in food uptake (17, 18) and a change in fly feeding preference depending on the missing macronutrients in its diet (19, 20). We assessed the impact of MSRO infection on fly feeding behavior with a FlyPad (18). Infected and uninfected flies given the choice between yeast (protein-rich diet) and sucrose (sugar-rich diet) showed no difference in the total number of sips on each source or in fly preference toward yeast over sucrose (Fig. 1*A* and *B*). We further assessed infected fly food uptake using two dye-based assays: the Capillary-Feeding (CAFE) assay, which measures liquid food uptake (21), and the Consumption-Excretion (ConEx) assay, which measures solid food uptake (22). Both methods confirmed that MSRO-infected flies did not increase their food uptake compared to their uninfected counterparts (Fig. 1*C* and *D*). Furthermore, a colorimetric food choice assay (19) did not detect any altered food preference between infected and uninfected flies, indicating that MSRO does not push its host to seek specific macronutrients (Fig. 1*E*). Last, we monitored starvation-induced locomotion, a behavioral response believed to foster foraging (23). Again, we observed no significant difference in locomotor activity of MSRO-infected flies compared to uninfected flies, indicating that they do not act like nutrient-deprived flies (Fig. 1*F*).

Collectively, these data robustly show that MSRO-infected flies do not increase or modify their foraging activity and food intake. As a consequence, nutrient availability in the hemolymph is likely similar whether the fly is infected or not, despite competition between fly tissues and MSRO.
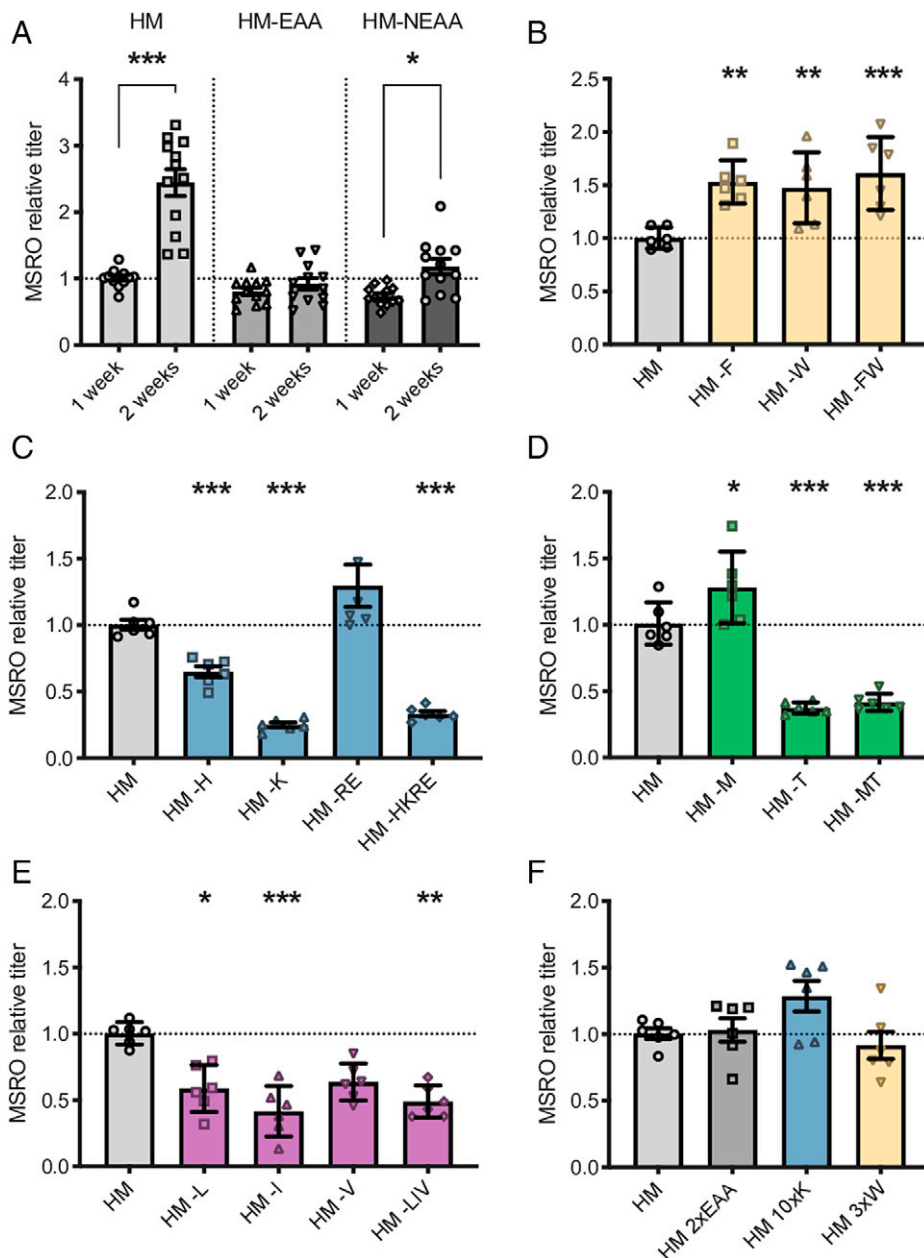
Fig. 2. Dietary availability of specific EAAs determines the ability of MSRO to grow in *Drosophila* hemolymph. (*A–F*) Each dot represents a biological replicate. Bars indicate the mean ± SEM of the MSRO titer measured by qPCR after 2 wk of *Drosophila* feeding on HM (light grey) depleted of EAAs (gray) or NEAAs (dark gray) (*A*), single EAA from the FW cluster (*B*), from the HKR(E) cluster (*C*), from the MT cluster (*D*), or from the LIV cluster (*E*) or supplemented with more EAAs, K or W (*F*). Titers are normalized to the HM control for each dataset. Horizontal dashed lines indicate the relative titer of controls (HM, 1). Data were analyzed by one-way ANOVA followed by Dunnett's multiple comparisons tests versus the complete HM. Asterisks indicate a statistically significant difference to the HM 1-wk control (gray on all graphs). *$P < 0.05$; **$P < 0.01$; ***$P < 0.001$.

2. MSRO Growth Mostly Relies on a Defined Subset of Host EAAs.

The absence of overt adaptation of the fly feeding behavior suggests that MSRO adapts its growth rate to available nutrients. Circulating DAGs are known to be limiting growth factors for MSRO (15); we theorized that other essential nutrients (i.e., nutrients that are required in the diet because fly tissues cannot synthesize them) could also be important limiting growth factors.

The *Spiroplasma* genus comprises host-associated species with poor anabolic capacities, especially regarding amino acids (*SI Appendix*, Fig. S1) (24). For example, the closely related species *Spiroplasma citri* requires supplementation of 18 out of 20 amino acids to grow properly (24). This prompted us to investigate amino acid requirements of *S. poulsonii* MSRO and, if applicable, which amino acids act as growth-limiting factors in the fly hemolymph.

To accurately determine the effects of specific amino acid depletion on MSRO growth, we employed holidic media (HM) to provide artificial diets of controlled chemical composition. We first assayed MSRO growth in flies raised on complete HM. We observed significant and reproducible MSRO growth in the hemolymph of flies that were born on normal medium and transferred to HM upon hatching (Fig. 2*A*).

We then depleted amino acid clusters from the HM based on *Drosophila* nutritional requirements (25): nonessential amino acids (NEAAs: A, C, D, E, G, N, P, Q, S, Y) that *Drosophila* can synthesize and EAAs (F, H, I, K, L, M, R, T, V, W) that must be derived from the diet. Weak but significant growth of MSRO was observed in the hemolymph of flies raised on HM depleted of NEAAs compared to the control HM, while growth was completely abolished in
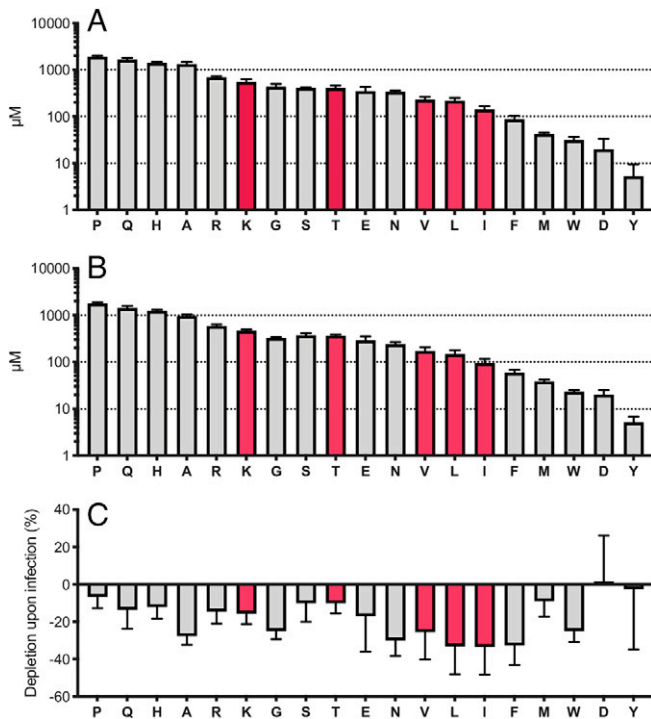
Fig. 3. MSRO EAA requirements do not correlate with their hemolymphatic availability.(*A* and *B*) Amino acid concentration in the hemolymph of uninfected (*A*) and MSRO-infected (*B*) flies. Red bars represent the five EAAs identified as limiting MSRO growth upon depletion in the fly's diet (K, L, I, T and V). Bars indicate the mean ± SD of four (*A*) or three (*B*) biological replicates. (*C*) Percentage of depletion of each amino acid upon MSRO infection, calculated as the ratio between the concentrations measured in the hemolymph of infected flies over that of uninfected flies. Bars indicate the mean± SD.

the absence of EAAs (Fig. 2*A*). This suggests that MSRO growth relies entirely on EAA presence in the fly diet, while NEAA depletion can be partially compensated for by fly anabolism.

We then investigated if specific EAA depletions had remarkable effects on MSRO growth. To this end, we depleted single EAAs or groups of EAAs with similar chemical properties and monitored MSRO growth. Of note, although arginine (R) is considered essential for *Drosophila* (25, 26), glutamate (E) can be used as a substrate for ornithine production, which is a precursor of arginine (27, 28). For this reason, we systematically depleted glutamate along with arginine. Surprisingly, depleting individual EAAs did not always impact MSRO growth as much as full EAA depletion did. Instead, depletion of different EAAs had specific impacts on MSRO growth. Both F and W single depletions increased MSRO titer (Fig. 2*B*). Depleting K alone was sufficient to recapitulate growth restriction induced by depletion of all EAAs (Fig. 2*C*). H depletion had a significant individual effect but was not sufficient to recapitulate the effect of full EAA or HKRE cluster depletion, indicating that it is required to a smaller extent than K. R depletion had no significant effect. T depletion stalled MSRO proliferation, while M depletion had no effect on growth (Fig. 2*D*). Among aliphatic amino acids, individual depletion of L and I significantly blocked MSRO growth (Fig. 2*E*). The effect of V depletion, although just missing statistical significance (Dunnett's multiple comparison test *P* value = 0.06), phenocopied that of the LIV cluster. Lastly, we monitored MSRO growth in flies raised on HM supplemented with EAAs (2-fold), K (10-fold), or W (3-fold) (Fig. 2*F*). We observed no growth difference compared with control HM, indicating that these EAAs are not limiting factors for MSRO growth when flies are well fed.

We concluded that MSRO growth strongly relies on the presence of only five EAAs in the host diet—K, L, I, T, and V, hereafter referred to as "KLITV"—and that these can be limiting for growth upon fly nutritional deprivation but not in well-fed conditions.

3. EAA Dependence of MSRO Is Not Correlated to EAA Abundance in the Hemolymph. The strong reliance of MSRO on only five EAAs out of 10 could be due to two nonexclusive hypotheses: 1) These EAAs could be scarce in the fly, such that depletion has a strong effect on MSRO growth compared to EAAs with larger stocks, and 2) these EAAs play a particular role in the physiology of bacteria and are critical for translating essential proteins. In the latter situation, even partial depletion would significantly affect MSRO growth.

In order to assess the availability of KLITV for MSRO, we performed a metabolomics analysis of hemolymph extracted from infected and uninfected flies raised on complete HM. Remarkably, (*S. poulsonii*) MSRO infection mildly depleted hemolymphatic amino acids (between −2% and −33% compared to uninfected flies; Fig. 3*C*). Furthermore, KLITV were not particularly rare in the hemolymph (Fig. 3 and Dataset S1). Upon infection, L and I were depleted by 33%, V by 25%, and K and T by only 16% and 10%, respectively (Fig. 3). F and W, whose artificial depletion in the diet promotes bacterial growth, respectively reached 32% and 25% depletion upon MSRO infection (Fig. 2*B*). This indicates that MSRO reliance on KLITV is not determined by their hemolymph availability when *Drosophila* is raised on a complete diet.

4. The Reliance of MSRO on K, L, I, V, and T Is Correlated to the Sequence and Abundance of the Membrane Lectin SpiB. We next sought to determine if KLITV were particularly abundant in the MSRO proteome. Using a previously published proteome of MSRO (29), we calculated the percentage of amino acid usage in the proteome based on sequence and abundance of each protein (Fig. 4*A*) and found that K, L, I, T, and V were the most represented EAAs in the total proteome. On the other hand, F, R, M, H, and W, whose depletion in the fly diet has no stalling effect on MSRO growth, are found at lower levels in the proteome. This indicates that MSRO dependence on precise EAAs is determined by specific bacterial needs rather than availability in the host hemolymph.

We next investigated whether specific proteins could drive MSRO EAA needs. For this, we calculated the fraction of the total pool of each amino acid allocated to the synthesis of the 20 most abundant proteins in the proteome (Fig. 4*B*). Only two proteins, SpiB and Fibril (Fib), were outliers in the total proteome because of their high abundance. Individually, SpiB demanded 22% of the total amino acid residues composing the proteome and Fib 6.6%. On top of its much higher abundance, SpiB also has a sequence in KLITV (49.5% of the sequence) that is richer than that of Fib (41% of the sequence). We therefore hypothesized that a disproportionate demand for KLITV allocated to SpiB production could be a limiting factor for bacterial growth upon depletion of these EAAs.

We then fitted linear models between the fraction of each EAA allocated to each of the three most abundant proteins and the effect of their depletion on MSRO growth (Fig. 4*C*). A goodness of fit of $R^2 = 0.3613$ was calculated for SpiB, versus 0.1255 and 0.0206 for the other two proteins, suggesting that EAA requirements for sustaining MSRO growth are largely dictated by the number of residues required to produce SpiB.
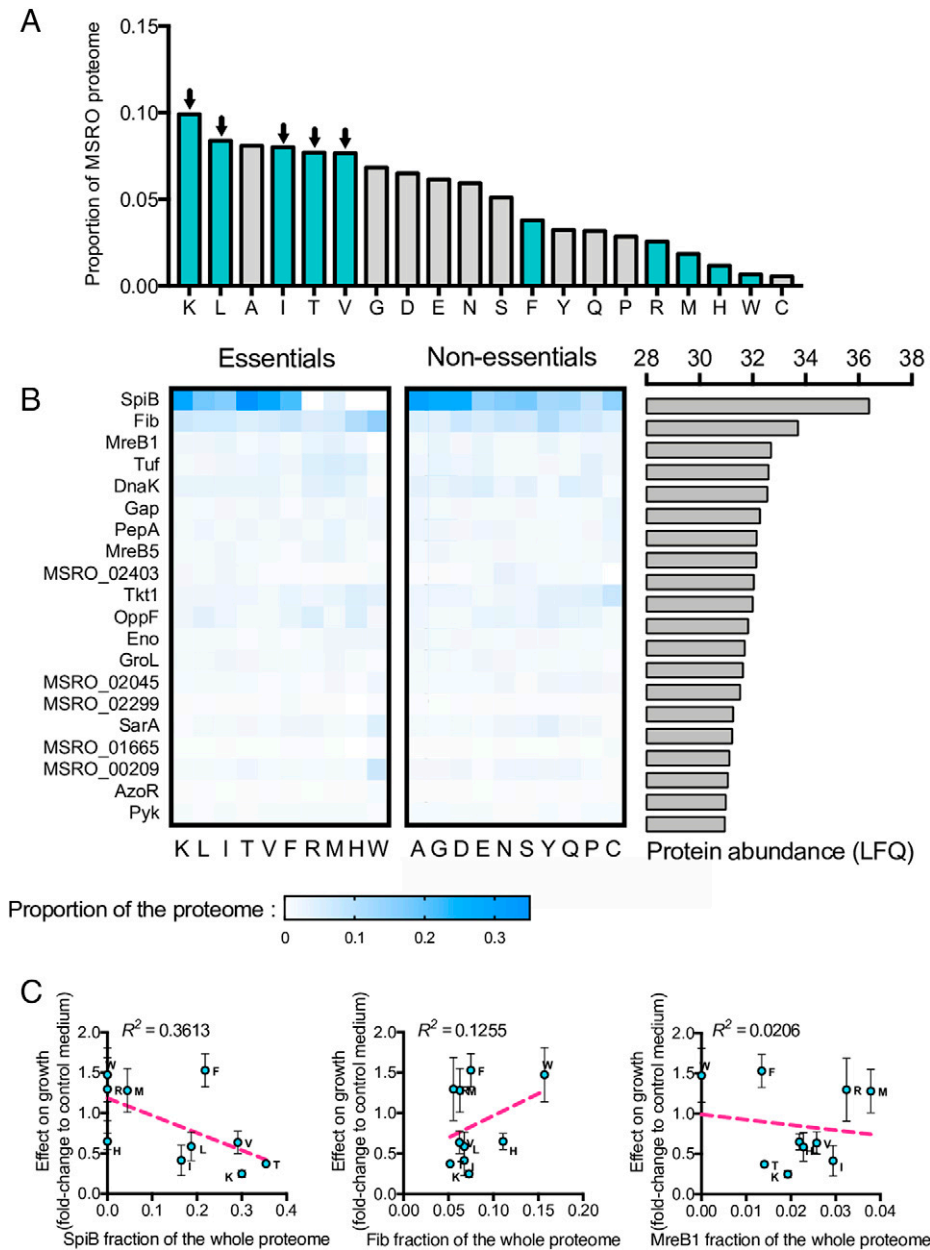
Fig. 4. SpiB abundance and composition determine MSRO EAA requirements. (*A*) Proportion of each amino acid composing the total proteome of MSRO, calculated from the protein sequence and abundance measured by LC-MS/MS. Blue bars indicate fly-EAAs, and black arrows highlight the five EAAs identified as limiting MSRO growth upon depletion in the fly's diet. (*B*) Amino acid allocation to the 20 most abundant proteins of MSRO. Gray bars represent the abundance published by Masson, Rommelaere et al. (29). (*C*) Correlations between the proportion of EAAs allocated to SpiB, Fib, and MreB1 and the effect of the corresponding depletion on MSRO growth. Each dot represents an amino acid, and bars represent SEM from Fig. 2. The pink dotted line represents a linear regression model with R^2 indicating the goodness-of-fit.

Collectively, these data indicate that SpiB sequence composition and extreme abundance may explain a large part of the growth phenotypes observed upon EAA depletions in the fly diet.

5. Depleting K, L, I, T, and V in the Fly Diet Specifically Affects SpiB Transcription and Translation. We next sought to experimentally validate the role of SpiB in driving MSRO reliance on specific EAAs. MSRO is a fastidious bacterium, and genomic knockouts remain unachievable. Therefore, we used *Drosophila* genetics to design a *spiB* heterologous expression tool, which we used to assess whether SpiB translation was affected by KLITV depletion. We ubiquitously overexpressed a secreted RFP (*UAS-secRFP*) or V5-tagged SpiB (*UAS-SpiB*) in uninfected flies and measured both their transcript and protein levels. We then used the ratio of protein signal over transcript

level to estimate the efficiency of their respective translation. We did not observe any differences in the ratios for RFP and SpiB when flies expressing the constructs were raised on a complete holidic diet. However, depletion of KLITV from the fly diet specifically reduced (although not significantly) SpiB translation, while RFP translation remained unchanged (Fig. 5*A*).

Spiralins are membrane lectins involved in *Spiroplasma* interaction with their hosts (30, 31). At least two isoforms have been described: SpiA is conserved across *Spiroplasma* species while SpiB is unique to MSRO. Although SpiAs from both *S. citri* and MSRO are also KLITV rich (46% and 51.6%, respectively), their abundance is much lower than that of SpiB (32, 33). We therefore hypothesized that MSRO growth would be more impacted by KLITV depletion than another *Spiroplasma* species, *S. citri*, which is devoid of SpiB. Indeed, we observed
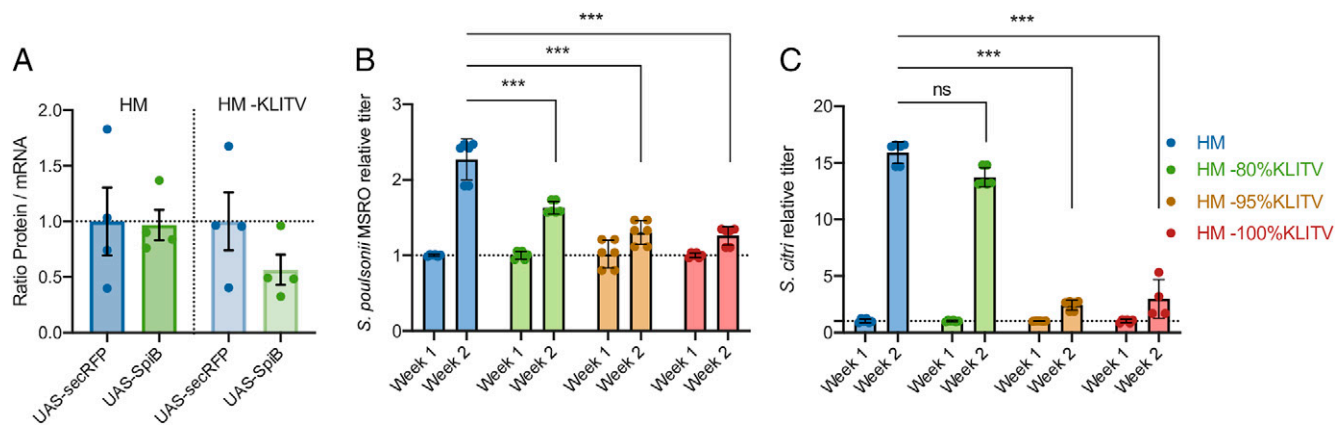
Fig. 5. SpiB expression affects fly translation and bacterial growth. (*A*) Ratio of the protein signal (measured by Western blot) over the transcription level (measured by qRT-PCR) of uninfected *Act5C-GAL4 > UAS-secRFP* and *Act5C-GAL4 > UAS-SpiB-V5* on complete HM or KLITV-depleted HM (HM-KLITV). Each dot represents a biological replicate. Bars indicate the mean ± SEM. Data were analyzed using Mann–Whitney *U* tests that revealed nonsignificant differences. (*B* and *C*) *S. poulsonii* MSRO titer (*B*) and *S. citri* titer (*C*) measured by qPCR after 1 or 2 wk of *Drosophila* feeding on complete HM (blue) or medium depleted of 80% (green), 95% (orange), or 100% (red) of KLITV. Each dot represents a biological replicate. Bars indicate the mean ± SEM. Relative titers are indicated as the fold change between the 2-wk measure and the 1-wk measure and as the copy number of the *Spiroplasma* gene *dnaK* over that of the host gene *rps17*. Data were analyzed by two-way ANOVA followed by Sidak's multiple comparisons tests. ns, not significant; ***$P < 0.001$. Horizontal dashed lines indicate the relative value of controls (1).

that a depletion of 80% of KLITV in the fly diet was sufficient to significantly decrease MSRO growth (Fig. 5*B*), while depletion of at least 95% was required to significantly stall *S. citri* growth (Fig. 5*C*).

Collectively, these results show that transcription and translation of SpiB are affected by dietary KLITV depletion and support the idea that SpiB is a limiting factor for *Spiroplasma* growth upon host EAA deprivation.

6. SpiB Is Likely to Be Required for Efficient Vertical Transmission of MSRO. The massive investment of MSRO in SpiB synthesis raised the question of its biological function. Since SpiB is absent in pathogenic species, which are horizontally transmitted, we hypothesized that it could be involved in the vertical transmission of endosymbiotic species.

In order to overcome the genetic intractability of MSRO, we assessed its vertical transmission efficiency in flies overexpressing a secreted version of SpiB (*Act5C-GAL4 > UAS-SpiB*). We reasoned that heterologous SpiB would saturate targets normally bound by bacterial SpiB and interfere with its function. We first assessed MSRO transmission by imaging the follicular epithelium of stage 10 egg chambers using confocal microscopy (Fig. 6*A*). Control flies displayed a very characteristic pattern of MSRO localized strictly at tricellular junctions between follicle cells (13). In contrast, flies overexpressing the secreted SpiB construct had a reduced MSRO signal and striking mislocalization of some bacteria between tricellular junctions, suggesting defective vertical transmission (Fig. 6*A* and *B*). Measurement of MSRO titers by qPCR and by immunofluorescence showed that eggs from mothers expressing secreted SpiB had strongly decreased bacterial titers compared to controls (Fig. 6*C* and *SI Appendix*, Fig. S2). This was accompanied by an increased bacterial titer in the mother's body, consistent with a reduced rate of vertical transmission.

In order to uncover the molecular interactants of SpiB, we proceeded to a coimmunoprecipitation experiment using SpiB as bait. Bound proteins were identified by liquid chromatography-tandem mass spectrometry (LC-MS/MS). This approach suggested only nine proteins as putative interactors of SpiB (Fig. 6*D* and Dataset S2). Remarkably, three of these proteins (Vml, Psd, and Yellow-g) are structural elements of the vitelline membrane (the first layer of the oocyte chorion) or participate in the

synthesis or maturation of the vitelline membrane, suggesting that SpiB may approximate MSRO to the egg, favoring its vertical transmission (34, 35).

Discussion

In this article, we investigated the amino acid requirements of the *Drosophila* facultative endosymbiont *S. poulsonii* MSRO. We found that MSRO growth relies on a specific subset of EAAs in the host diet, which correlates with its requirements for SpiB translation.

Our first observation is that young MSRO-infected flies do not display any starvation-induced behaviors, such as increased food uptake or oriented food choice toward protein-rich food, suggesting that they are not nutritionally disadvantaged by the infection. This observation is confirmed by hemolymph metabolomics, which shows that MSRO depletes between 0% and 33% of the amino acid amounts measured in uninfected flies. Hence, in well-fed flies, MSRO metabolism does not cause significant amino acid deprivation. MSRO growth stalling upon EAA depletion in the fly diet further suggests that the host has the upper hand in competition for amino acids, regardless of their effective availability in the diet.

Based on our results, amino acids can be classified in three groups depending on their effect on MSRO growth.

The first group has no or little effect on MSRO growth when depleted. This includes NEAAs, the depletion of which is most likely compensated by fly anabolism, but also the EAAs R and M. Remarkably, these two amino acids are completely absent in the SpiB sequence (with the exception of the initial M). In order to ensure proper development, larval growth was achieved on a standard *Drosophila* diet. As a consequence, adults retained larval stocks of amino acids when they were transferred to depleted media. Since MSRO does not require M and R for SpiB synthesis, the host larval stocks likely covered the remaining needs, which could explain their lack of effect on MSRO growth within our 2-wk experimental time frame.

The second group, composed of F and W only, had a positive impact on MSRO growth when depleted in the fly diet. This result is surprising as these amino acids are not known to be directly toxic for cells at physiological concentrations. They could, however, serve as a precursor for toxic compounds
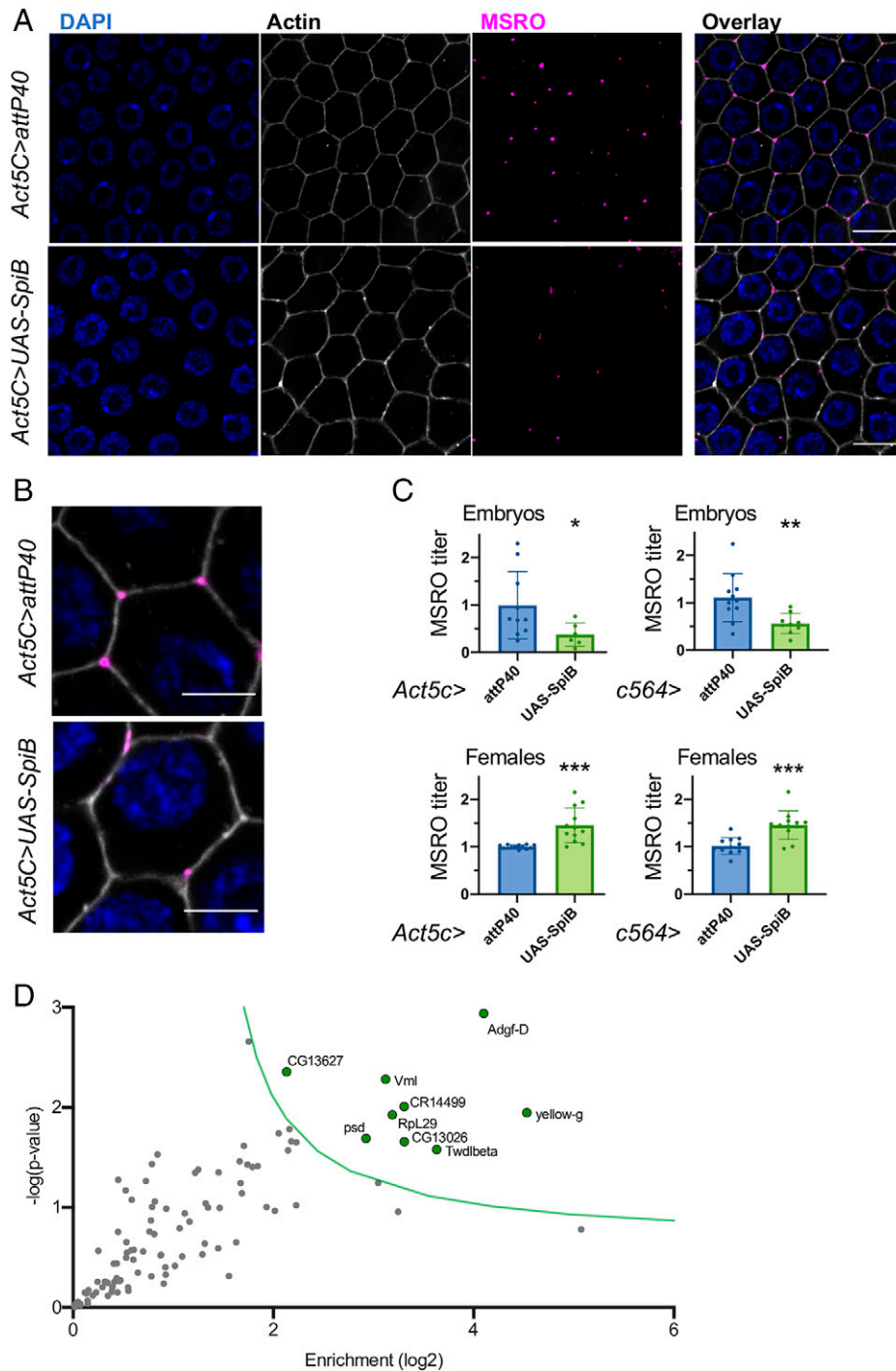
Fig. 6. SpiB participates in MSRO vertical transmission. (A) Representative images of the follicular epithelium of stage 10 egg chambers from MSRO-infected flies. Genotypes are indicated on the left for each row. Scale bar, 10 μm. Image brightness and contrast have been adjusted for better readability. (B) Zoom of a group of tricellular junctions from A showing the mislocalization of MSRO upon expression of UAS-SpiB by the host. Scale bar, 5 μm. (C) qPCR quantification of MSRO in mothers and eggs of lines expressing the UAS-SpiB construct. Each dot represents a biological replicate, and bars represent the mean ± SD. Statistical significance was assessed using unpaired t tests. *$P < 0.05$; **$P < 0.01$; ***$P < 0.001$. (D) Volcano plot of SpiB-V5 interactors identified by coimmunoprecipitation. Each dot represents a single protein. Significance of the interaction is indicated by the green dots, for proteins with FDR > 0.05, and s0 (green line) = 1.

produced either by the fly or by MSRO itself. Alternatively, these amino acids or their derivatives could act as signaling molecules that negatively regulate bacterial proliferation.

The third and last group, comprising KLITV, completely abolished MSRO growth when absent in the fly diet. We cannot exclude an indirect effect on MSRO growth caused by the impact of these depletions on the fly physiology. However, we showed that these specific EAAs, particularly K and T, were required in high amounts for synthesis of the membrane lectin

SpiB, which prompted us to instead consider a direct effect on the bacterial physiology, with a connection with this protein specifically. The effect of KLITV limitation on bacterial growth could result from different mechanisms: 1) Reduced SpiB synthesis may directly stall proliferation if SpiB is essential to MSRO growth, or 2) the extreme abundance of SpiB protein and *spiB* transcripts in MSRO (36) suggests that SpiB synthesis monopolizes the translation machinery, including ribosomal machinery and transfer RNA (tRNA)-charged amino acids.

The availability of tRNA-charged amino acids determines translation efficiency at the cell level (37, 38), and imbalance in the pool of tRNA-charged amino acids causes cellular stress and translation errors (39, 40). Hogging of tRNAs charged with KLITV by SpiB translation could generate global translational stress and reduce the availability of these amino acids for synthesis of other proteins, including core proteins involved in essential cellular functions.

The extreme abundance of SpiB favors the interpretation that SpiB itself is critical. In MSRO, SpiB alone accounts for 32% of the total protein count and 22% of amino acid requirements. For comparison, the most abundant proteins in *Escherichia coli* (the major outer membrane lipoprotein Lpp) and the Mollicute *Mycoplasma pneumoniae* (the translation elongation factor Tuf) account for only 2.8% and 3.7% of the total proteome, respectively (41). In algae, where the photosynthetic machinery represents over 20% of the protein amount in one cell, no single protein surpasses 6% of the total proteome (42). The extreme abundance of SpiB is therefore a remarkable case among both prokaryotes and eukaryotes.

In *S. citri,* SpiA is a membrane lectin required for adhesion to insect cells and horizontal transmission to plants (43). However, it is dispensable for cell growth, survival, and motility (31). Our results strongly suggest that SpiB is required for efficient vertical transmission of endosymbiotic *Spiroplasma*, reminiscent of SpiA function in *S. citri.* Although the lack of genetic tools on MSRO prevents any definitive demonstration, the similarities between the two proteins suggest that SpiB may be dispensable at the level of a single bacterial cell but is likely necessary to maintain interaction with the host over evolutionary time through vertical transmission.

Previous work indicates that MSRO transmission happens during vitellogenesis (stage 10) and relies on massive endocytosis triggered by the recognition of Yolk Protein 1 (YP1) by the oocyte membrane receptor Yolkless (Yl) (13). However, the exact molecular determinants of vertical transmission remain uncharacterized. Our results show that SpiB interacts with the maternally loaded proteins Vml and Psd. Importantly, these proteins are both involved in the synthesis of the vitelline membrane (the first layer of the oocyte chorion) (34, 35), which is morphologically complete at stage 11 (44). Both proteins are glycosylated, which is consistent with a possible interaction with the lectin domain of SpiB (34, 35). Previous work and single-cell RNA sequencing data (45) indicate that they are expressed by follicle cells between stages 10 and 11, concomitant with MSRO oocyte invasion. These observations led us to hypothesize that at least one of these two proteins could bring MSRO to the oocyte and allow vertical transmission in a two-step process. First, interaction of Vml and/or Psd with SpiB on the bacterial membrane would direct the bacteria through the follicular epithelium toward the oocyte. Then, bacteria intercalated between the follicle cells and oocyte membrane would be taken up into oocyte yolk granules by YP1-Yl–mediated endocytosis, along with YP1 and other maternal materials. SpiB interaction with Vml and/or Psd could thus ensure MSRO entry into the oocyte at an optimal time, when the oocyte is as mature as possible but before chorion synthesis seals it and prevents further bacterial entry.

Collectively, our data highlight SpiB as a major regulator of MSRO–*Drosophila* symbiotic homeostasis. The dominance of SpiB in the MSRO proteome emphasizes the massive investment of the bacteria in this protein and, consequently, toward efficient vertical transmission. Intriguingly, SpiB regulates both efficient vertical transmission and proliferation of MSRO in the fly hemolymph. These two key aspects of MSRO physiology are thereby linked by a single endosymbiont protein to EAA availability in the hemolymph and thus to the nutritional status of the host. We propose that SpiB synthesis acts as a metabolic bottleneck, promoting transmission while preventing MSRO overgrowth in young fertile flies and ensuring stability of the interaction over evolutionary time even in nutrient-scarce conditions.

Materials and Methods

***Spiroplasma* and *Drosophila* Stocks.** OregonR flies were raised at 25 °C on cornmeal medium (35.28 g cornmeal, 35.28 g inactivated yeast, 3.72 g agar, 36 mL fruit juice, 2.9 mL propionic acid, and 15.9 mL Moldex for 600 mL of medium). MSRO-infected females were transferred to HM within a day of emergence and mated with OregonR males. Fly stocks were infected by *S. poulsonii* MSRO Uganda-1 several years prior to the experiments as previously described (46). Briefly, 9 nL MSRO-infected hemolymph was injected into the thorax. The progeny of these flies was collected after 5 to 7 d using male killing as a proxy to assess the infection (100% female progeny). *S. citri* GII-3 was cultured in SP4 medium at 32 °C. Infections were carried out by injecting 9 nL of overnight culture diluted threefold in phosphate-buffered saline (PBS) in the thorax of 3- to 4-d-old females using a Nanoject II (Drummond).

The following fly stocks were purchased from Bloomington *Drosophila* Stock Center: *Act5C-GAL4* (#4414), *C564-GAL4* (#6982), attP40 (36304), and VK33 (#9750). *UAS-secRFP* was kindly provided by J. Pastor-Pareja (Peking-Tsinghua Center for Life Sciences, Beijing 100084, China)(47). UAS-SpiB was constructed according to the following steps using Geneious Prime software 2021.2.2 (Biomatters Limited). The MSRO SpiB coding sequence (GenBank reference No. SMSRO_RS04040) was trimmed to keep nucleotides 51 to 795, corresponding to the coding part without the predicted signal peptide and stop codon. The signal peptide of *D. melanogaster* Turandot A (coding for the first 23 amino acids of GenBank reference NP_536778.2) was added directly upstream of *spiB*. A (GGGS)₃ linker, followed directly by the 69 bp of the V5-6xHis tag from pUAST-attB-GFP-V5-His plasmid (Addgene #85621), which were added downstream of *spiB*. The whole construct was codon-optimized for translation in *D. melanogaster* using Genewiz proprietary algorithm and ordered as a total synthesis from Genewiz Germany GmbH. The fragment was inserted into pUAST-attB-GFP-V5-His between positions 262 and 1,140 of the plasmid sequence (thereby replacing the GFP-V5-His tag) using Gibson Assembly Master Mix from New England Biolabs) following manufacturer's instructions. The construct was microinjected in VK33 attP embryos.

HM. HM was prepared as previously described (26) with some modifications. The acetate buffer was not included in the autoclaved base to prevent acidic lysis of the agar. The concentration of all nonautoclaved components was reduced to 70% of the original recipe. Depletion of amino acids was compensated by addition of water when required. Media were stored at 4 °C and used for a maximum of 10 d.

Feeding Behavior. Feeding behavior was assessed on infected or uninfected 7- to 10-d-old OregonR females mated shortly after emergence with OregonR males. The FlyPad was used as previously described (18). Briefly, flies were starved on 1% agarose for 1 h at 29 °C and individually put in arenas with a choice between 10% yeast or 20 mM sucrose in 1% agarose. Feeding activity and preference were recorded and analyzed by FlyPad software using default parameters. The experiment was repeated three times, with independent batches of 24 flies for each infection condition. The CAFE and ConEx assays were performed strictly as previously described on six independent replicates of five flies (21, 22). *Drosophila* Activity Monitor (DAM) assays were performed as previously described on 2.5% sucrose (48) on three independent batches of 32 flies for each infection condition. Food choice assays were performed 12 independent times on 20 females as previously described (20) without CO_2 anesthesia and with amaranth 5 μg/mL instead of erythrosine B to color the food red.

***Spiroplasma* Quantification by qPCR.** *Spiroplasma* quantification by qPCR was performed as previously described (49). Briefly, the DNA was extracted from pools of five whole flies or 40 0- to 2-h-old embryos. The copy number of the single-copy bacterial gene *dnaK* was quantified and normalized to that of the

host gene *rsp17*. Primer sequences are available in *SI Appendix*, Table S1. Each experiment was repeated two or three independent times with at least three replicates each. Data analysis was adapted to each experimental design and is described in the figure legends.

***Spiroplasma* Quantification by Immunofluorescence.** Two independent samples of hemolymph were extracted from three female flies by tearing their abdomen with forceps and mixed with 100 µL of PBS containing 30 µM Hoechst 33343 (cat. H3570, Thermo Fisher Scientific). The suspension was then deposited on an agarose pad, and 10 random fields of view were imaged immediately under a fluorescent microscope (Axio Imager Z1, Zeiss). MSRO quantification was performed on ImageJ version 2.1.0/1.53C by manually thresholding each picture and counting particles larger than 10 px (exclude on edge, no circularity criteria).

Embryos were collected 0 to 5 h after egg laying and dechorionated with 7% bleach for 90 s. Embryos were then fixed 20 min in 50% heptane:4% formaldehyde in PBS and devitellinized by vigorous shaking in methanol:heptane (1:1). Embryos were stained for DNA (4′,6-diamidino-2-phenylindole [DAPI]) and MSRO (immunofluorescence) following the same procedure as for ovaries (see below), mounted, and observed on a Zeiss LSM700 confocal microscope. Stacks of 24 embryos from two independent replicates were acquired with 1-µm spacing. On a maximum projection of each stack, MSRO was quantified as the ratio between the percentage of the image covered by MSRO signal over the percentage of the image covered by DAPI signal (approximating the surface of the embryo).

qRT-PCR. Gene expression was measured by qRT-PCR as previously described (50). Briefly, 10 whole flies were crushed, and their RNA was extracted with the TRIzol method. DNA degradation was performed using deoxyribonuclease I (Thermo Fisher Scientific). RT was carried out using a PrimeScript RT kit (Takara) and a mix of random hexamers and oligo-dTs. qPCR was performed on a QuantStudio 3 (Applied Biosystems) with PowerUp SYBR Green Master Mix using primer sequences available in *SI Appendix*, Table S1. The expression of the target gene was normalized to that of the housekeeping gene *rp49* (*rpL32*) using the delta-delta-CT (ΔΔCT) method (51). Each experiment was repeated two or three independent times with at least three technical replicates each. Data were analyzed by one-way ANOVA followed by Dunnett's multiple comparisons.

Proteome Analyses. The proteome analyses were based on a previously published *S. poulsonii* MSRO proteome (29). The relative amino acid allocation to each protein was calculated by multiplying the $2^{(\text{LabelFreeQuantification})}$ (2^{LFQ}) value by the number of corresponding residues in the primary sequence of the protein. The proportion of each amino acid in the whole proteome was obtained by summing the residue allocation of all proteins. The relative abundance of SpiB was calculated by dividing the 2^{LFQ} value of the protein by the sum of 2^{LFQ} values of all detected proteins.

Western Blot. Ten flies were homogenized in RIPA buffer supplemented with protease inhibitors using a Precellys 24 homogenizer (Bertin Technologies). Homogenates were spun 10 min at $1,000 \times g$, and supernatants were centrifuged 30 min at $13,000 \times g$ at 4 °C. Protein concentration of the samples was determined by bicinchoninic acid assay (BCA) assay, and 30 µg of protein extract was separated on a 4 to 12% acrylamide precast Novex NuPage gel (Invitrogen) under reducing conditions and transferred to nitrocellulose membranes (Invitrogen iBlot). After blocking in 5% nonfat dry milk in PBS containing 0.1% Tween-20 for 1 h, membranes were incubated at 4 °C overnight with a rabbit anti-RFP antibody (Abcam, #ab62341) in a 1:1,000 dilution, a mouse anti–α-Tubulin (Sigma-Aldrich, #T6199) in a 1:1,000 dilution, or a rabbit anti-V5 antibody (Invitrogen, #V8137) in a 1:1,000 dilution. Donkey anti–mouse-HRP or anti–rabbit-HRP secondary antibody (Jackson ImmunoResearch) in a 1:15,000 dilution was incubated for 45 min at room temperature. Bound antibody was detected using ECL (GE Healthcare) according to the manufacturer's instructions. Membranes were imaged on a Fusion FX7 (Vilber), and band intensity was quantified using ImageJ software. Protein over messenger RNA (mRNA) ratios were calculated as follows: The band intensity of the RFP or V5 (Spiralin) signal was normalized to that of Tubulin to obtain a normalized protein signal. The protein signal was divided by the expression level of the construct (see qRT-PCR paragraph) to obtain the protein/mRNA ratio. Ratios were then normalized to that of the RFP construct.

Immunostaining. Ovaries were dissected in PBS, and fixed for 1 h at room temperature in 4% paraformaldehyde in PBS under shaking. Tissues were subsequently rinsed in PBS with 0.1% Triton X-100 (PBT), permeabilized for 1 h in PBT with shaking, and blocked in 2% bovine serum albumin in PBT for 1 h with shaking. Tissues were incubated with primary antibodies in 2% bovine serum albumin in PBT overnight at 4 °C with shaking. After 1-h washing in PBT, secondary antibodies and DAPI were applied at room temperature for 2 h and washed for 1 h in PBT, and the tissues were mounted in fluorescence mounting medium (Dako). Primary antibodies are as follows: mouse anti-RFP (Abcam, #ab62341, 1:500), rabbit serum anti-MSRO [(13), 1:300], and anti-V5 tag (Thermo Fisher Scientific, #25F11F7, 1:500). Alexa488- or Alexa555-conjugated secondary antibodies (Life Technologies) were used at 1:1,000. Alexa647 Phalloidin (Life Technologies) was used to stain F-actin (1:200). All images were taken on a Zeiss LSM 700 confocal microscope and processed using ImageJ.

Amino Acid Quantification. Using a Nanoject II (Drummond), 1.5 µL of hemolymph was extracted from uninfected or MSRO-infected females aged 7 to 10 d. Hemolymph was diluted on ice in 9 µL of PBS containing 1 nM *N*-Phenylthiourea (Sigma-Aldrich) and frozen immediately to prevent degradation. Four replicates per condition were used. A 10-µL sample was mixed with 40 µL 0.1% formic acid in water and 250 µL methanol containing isotopic-labeled internal standards (ISs). Sample extracts were vortexed and centrifuged (15 min, $2,700 \times g$ at 4 °C). The resulting supernatant was collected and injected into the liquid chromatography–mass spectrometry system for amino acid quantification.

A Vanquish Horizon (Thermo Fisher Scientific) ultra-high–performance liquid chromatography system coupled to Q-Exactive Focus interfaced with an HESI source was used for the quantification of amino acids. Chromatographic separation was carried out using an Acquity BEH Amide (1.7 µm, 100 mm × 2.1 mm I.D.) column (Waters). The mobile phase was composed of A = 20 mM ammonium formate and 0.1% formic acid in water and B = 0.1% formic acid in acetonitrile. The gradient elution started at 95% B (0 to 2 min), decreasing to 65% B (2 to 14 min) and reaching 50% B at 16 min, and was followed by an isocratic step (16 to 18 min) before a 4-min postrun for column reequilibration. The flow rate was 400 µL/min, the column temperature was 25 °C, and the sample injection volume was 2 µL. Heated Electrospray Ionization source conditions operating in positive mode were set as follows: sheath gas flow at 60, aux gas flow rate at 20, sweep gas flow rate at 2, spray voltage at +3 kV, capillary temperature at 300 °C, s-lens RF level at 60, and aux gas heater temperature at 300 °C. Full-scan high resolution mass spectrometry acquisition mode (*m/z* 50 to 750) was used with the following MS acquisition parameters: resolution at 70,000 full-width at half-maximum (FWHM), 1 microscan, 1e6 Automated Gain Control, and 100 ms as maximum inject time.

Data were processed using Xcalibur (version 4.1, Thermo Fischer Scientific). For absolute quantification, calibration curves and stable isotope-labeled ISs were used to determine the response factor. Linearity of the standard curves was evaluated for each metabolite using a nine-point range; in addition, peak area integration was manually curated and corrected where necessary. Concentrations of the compounds for which the ISs were available were corrected for the ratio of mass spectrometry (MS) response (peak area) between the analyte and the IS to account for matrix effects.

Sample Preparation for MS. A volume of 25 µL anti-V5 Magnetic Beads slurry (Chromotek) was used for each immune-precipitation following the manufacturer's instruction. Briefly, beads were washed with 180 µL PBS-0.1%Tween 20 (PBS-T), then saturated for 20 min with 2% bovine serum albumin in PBS-T. Ten female flies were homogenized in 300 µL Lysis Buffer (50 mM Tris, pH 8.5, 150 mM NaCl, and 1% TritonX-100 supplemented with 2X Protease inhibitor mixture [Roche]) and incubated on ice for 30 min. Protein extracts were centrifuged 10 min at 15,000 rpm and incubated with the beads for 1 h at room temperature on a carousel. Beads were washed three times with PBS-T and boiled in Laemmli buffer at 95 °C for 10 min. Subsequent MS-based proteomics-related experiments were performed by the Proteomics Core Facility at École Polytechnique Fédérale de Lausanne.

Protein samples were loaded on a sodium dodecyl sulfate polyacrylamide gel electrophoresis gel and allowed to briefly migrate. The gel pieces containing the concentrated proteins were excised and washed twice with 50% ethanol in 50 mM ammonium bicarbonate (AB; Sigma-Aldrich) for 20 min and dried by vacuum centrifugation. Proteins were reduced with 10 mM dithioerythritol (Merck-Millipore) for 1 h at 56 °C followed by a washing-drying step as

described above. Reduced proteins were alkylated with 55 mM Iodoacetamide (Sigma-Aldrich) for 45 min at 37 °C in the dark, followed by a washing-drying step as described above. Proteins were digested overnight at 37 °C using MS-grade Trypsin gold (Typsin Gold, Promega) at a concentration of 12.5 ng/µL in 50 mM AB supplemented with 10 mM CaCl$_2$. Resulting peptides were extracted in 70% ethanol, 5% formic acid (FA; Merck-Millipore) twice for 20 min, dried by vacuum centrifugation, and stored at −20 °C until further analysis.

MS. Peptides were desalted on C18 StageTips (52) and dried by vacuum centrifugation prior to LC-MS/MS injections. Samples were resuspended in 2% acetonitrile (Biosolve) and 0.1% FA, and nano-flow separations were performed on a Dionex Ultimate 3000 RSLC nano UPLC system (Thermo Fisher Scientific) online connected with an Orbitrap Lumos Fusion Mass-Spectrometer (Thermo Fisher Scientific). A capillary precolumn (Acclaim Pepmap C18, 3 µm-100 Å, 2 cm × 75 µm I.D.) was used for sample trapping and cleaning. A 50-cm-long capillary column (75 µm I.D.; in-house packed using ReproSil-Pur C18-AQ 1.9-µm silica beads; Dr. Maisch) was then used for analytical separations at 250 nL/min over 90-min biphasic gradients. Acquisitions were performed through Top Speed Data-Dependent acquisition mode using a cycle time of 2 s. First MS scans were acquired with a resolution of 60,000 (at 200 m/z), and the most intense parent ions were selected and fragmented by high-energy collision dissociation with a normalized collision energy of 30% using an isolation window of 1.4 m/z. Fragmented ions were acquired with a resolution of 15,000 (at 200 m/z), and selected ions were then excluded for the following 20 s.

Raw data were processed using MaxQuant 1.6.10.43 (53) against the Uniprot Reference Proteome of *D. melanogaster* (UP000000803) and of *S. poulsonii* MSRO (UP000031565) databases. Carbamidomethylation was set as fixed modification, whereas oxidation (M), phosphorylation (S, T, Y), acetylation (Protein *N*-term), CAMthiopropanoyl (K and Protein *N*-term), and glutamine to pyroglutamate were considered as variable modifications. A maximum of two missed cleavages was allowed, and "Match between runs" option was enabled. A minimum of two peptides was required for protein identification, and the

false discovery rate (FDR) cutoff was set to 0.01 for both peptides and proteins. Label-free quantification and normalization were performed by Maxquant using the MaxLFQ algorithm with the standard settings (54).

The statistical analysis was performed using Perseus version 1.6.12.0 (55) from the MaxQuant tool suite. Reverse proteins, potential contaminants, and proteins only identified by sites were filtered out. Protein groups containing at least two valid values in at least one group were conserved for further analysis. Empty values were imputed with random numbers from a normal distribution (width: 0.4 and down shift: 1.8 SD). A two-sample t test with permutation-based FDR statistics (250 permutations, FDR = 0.05, S0 = 1) was performed to determine significant differentially abundant candidates.

Statistical Analyses. Each experiment was repeated independently a minimum of three times (unless otherwise indicated), and error bars represent the mean and SE. Data were analyzed using appropriate statistical tests as indicated in the figure legends using GraphPad Prism software. P values are represented in the figures by the following symbols: *, P value < 0.05; **, P value < 0.01; and ***, P value < 0.001.

Data Availability. All data are included in the manuscript and/or supporting information.

Author affiliations: [a]Global Health Institute, School of Life Sciences, École Polytechnique Fédérale de Lausanne, Lausanne, 1015 Switzerland

1. A. E. Douglas, Multiorganismal insects: Diversity and function of resident microorganisms. *Annu. Rev. Entomol.* **60**, 17–34 (2015).
2. M. McFall-Ngai et al., Animals in a bacterial world, a new imperative for the life sciences. *Proc. Natl. Acad. Sci. U.S.A.* **110**, 3229–3236 (2013).
3. F. Masson, B. Lemaitre, Growing ungrowable bacteria: Overview and perspectives on insect symbiont culturability. *Microbiol. Mol. Biol. Rev.* **84**, e00089-20 (2020).
4. O. Duron et al., The diversity of reproductive parasites among arthropods: *Wolbachia* do not walk alone. *BMC Biol.* **6**, 27 (2008).
5. P. Medina, S. L. Russell, K. Aswadhati, R. Corbett-Detig, Deep data mining reveals variable abundance and distribution of microbial reproductive manipulators within and among diverse host species. bioRxiv [Preprint] (2020). https://doi.org/10.1101/679837. Accessed November 2021
6. G. D. D. Hurst, C. L. Frost, Reproductive parasitism: Maternally inherited symbionts in a biparental world. *Cold Spring Harb. Perspect. Biol.* **7**, a017699 (2015).
7. J. H. Werren, L. Baldo, M. E. Clark, *Wolbachia*: Master manipulators of invertebrate biology. *Nat. Rev. Microbiol.* **6**, 741–751 (2008).
8. L. M. Hedges, J. C. Brownlie, S. L. O'Neill, K. N. Johnson, *Wolbachia* and virus protection in insects. *Science* **322**, 702 (2008).
9. L. Teixeira, A. Ferreira, M. Ashburner, The bacterial symbiont *Wolbachia* induces resistance to RNA viral infections in *Drosophila melanogaster*. *PLoS Biol.* **6**, e2 (2008).
10. A. A. Hoffmann, P. A. Ross, G. Rašić, *Wolbachia* strains for disease control: Ecological and evolutionary considerations. *Evol. Appl.* **8**, 751–768 (2015).
11. G. E. Gasparich, C. Kuo, X. Foissac, "Spiroplasma" in *Bergey's Manual of Systematics of Archaea and Bacteria* (Wiley, 2020), pp. 1–52.
12. M. Mateos et al., Heritable endosymbionts of Drosophila. *Genetics* **174**, 363–376 (2006).
13. J. K. Herren, J. C. Paredes, F. Schüpfer, B. Lemaitre, Vertical transmission of a *Drosophila* endosymbiont via cooption of the yolk transport and internalization machinery. *MBio* **4**, e005 (2013).
14. Y. Niki, Ultrastructural study of the sex ratio organism (SRO) transmission into oocytes during oogenesis in *Drosophila melanogaster*. *Jpn. J. Genet.* **63**, 11–21 (1988).
15. J. K. Herren et al., Insect endosymbiont proliferation is limited by lipid availability. *eLife* **3**, e02964 (2014).
16. A. Marra, F. Masson, B. Lemaitre, The iron transporter Transferrin 1 mediates homeostasis of the endosymbiotic relationship between *Drosophila melanogaster* and *Spiroplasma poulsonii*. *microLife* **2**, uqab008 (2021).
17. R. Yapici, R. Cohn, C. Schusterreiter, V. Ruta, L. B. Vosshall, A taste circuit that regulates ingestion by integrating food and hunger signals. *Cell* **165**, 715–729 (2016).
18. P. M. Itskov et al., Automated monitoring and quantitative analysis of feeding behaviour in Drosophila. *Nat. Commun.* **5**, 4560 (2014).
19. C. Ribeiro, B. J. Dickson, Sex peptide receptor and neuronal TOR/S6K signaling modulate nutrient balancing in *Drosophila*. *Curr. Biol.* **20**, 1000–1005 (2010).
20. R. Leitão-Gonçalves, Commensal bacteria and essential amino acids control food choice behavior and reproduction. *PLoS Biol.* **15**, e2000862 (2017).
21. W. W. Ja et al., Prandiology of *Drosophila* and the CAFE assay. *Proc. Natl. Acad. Sci. U.S.A.* **104**, 8253–8256 (2007).
22. B. C. Shell et al., Measurement of solid food intake in *Drosophila* via consumption-excretion of a dye tracer. *Sci. Rep.* **8**, 11536 (2018).
23. G. Lee, J. H. Park, Hemolymph sugar homeostasis and starvation-induced hyperactivity affected by genetic manipulations of the adipokinetic hormone-encoding gene in Drosophila melanogaster. *Genetics* **167**, 311–323 (2004).
24. A. Patterson, C. Stevens, R. Cody, R. Gudauskas, Differential amino acid utilization by Spiroplasmas and the effect on growth kinetics. *J. Gen. Appl. Microbiol.* **31**, 499–505 (1985).
25. J. Consuegra et al., *Drosophila*-associated bacteria differentially shape the nutritional requirements of their host during juvenile growth. *PLoS Biol.* **18**, e3000681 (2020).
26. M. D. W. Piper et al., Matching dietary amino acid balance to the in silico-translated exome optimizes growth and reproduction without cost to lifespan. *Cell Metab.* **25**, 610–621 (2017).
27. K. M. Yoshida, N. Juni, S. H. Hori, Molecular cloning and characterization of *Drosophila* ornithine aminotransferase gene. *Genes Genet. Syst.* **72**, 9–17 (1997).
28. G. Ventura et al., Overexpression of ornithine aminotransferase: Consequences on amino acid homeostasis. *Br. J. Nutr.* **101**, 843–851 (2009).
29. F. Masson, S. Rommelaere, A. Marra, F. Schüpfer, B. Lemaitre, Dual proteomics of *Drosophila melanogaster* hemolymph infected with the heritable endosymbiont *Spiroplasma poulsonii*. *PLoS One* **16**, e0250524 (2021).
30. N. Killiny, M. Castroviejo, C. Saillard, *Spiroplasma citri* Spiralin acts in vitro as a lectin binding to glycoproteins from its insect vector *Circulifer haematoceps*. *Phytopathology* **95**, 541–548 (2005).
31. S. Duret, N. Berho, J. L. Danet, M. Garnier, J. Renaudin, Spiralin is not essential for helicity, motility, or pathogenicity but is required for efficient transmission of *Spiroplasma citri* by its leafhopper vector *Circulifer haematoceps*. *Appl. Environ. Microbiol.* **69**, 6225–6234 (2003).
32. H. Wróblewski, K.-E. Johansson, S. Hjérten, Purification and characterization of spiralin, the main protein of the *Spiroplasma citri* membrane. *Biochim. Biophys. Acta* **465**, 275–289 (1977).
33. J. C. Paredes et al., Genome sequence of the *Drosophila melanogaster* male-killing *Spiroplasma* strain MSRO endosymbiont. *MBio* **6**, 1–12 (2015).
34. Z. Zhang, L. M. Stevens, D. Stein, Sulfation of eggshell components by Pipe defines dorsal-ventral polarity in the *Drosophila* embryo. *Curr. Biol.* **19**, 1200–1205 (2009).
35. M. Elalayli, J. Palisade is required in the *Drosophila* ovary for assembly and function of the protective vitelline membrane. *Dev. Biol.* **319**, 359–369 (2008).
36. F. Masson, S. Calderon Copete, F. Schüpfer, G. Garcia-Arraez, B. Lemaitre, In vitro culture of the insect endosymbiont *Spiroplasma poulsonii* highlights bacterial genes involved in host-symbiont interaction. *MBio* **9**, e000 (2018).
37. A. L. Starosta, J. Lassak, K. Jung, D. N. Wilson, The bacterial translation stress response. *FEMS Microbiol. Rev.* **38**, 1172–1201 (2014).
38. S. Varenne, J. Buc, R. Lloubes, C. Lazdunski, Translation is a non-uniform process. Effect of tRNA availability on the rate of elongation of nascent polypeptide chains. *J. Mol. Biol.* **180**, 549–576 (1984).
39. Z. Bloom-Ackermann et al., A comprehensive tRNA deletion library unravels the genetic architecture of the tRNA pool. *PLoS Genet.* **10**, e1004084 (2014).
40. D. D. Nedialkova, S. A. Leidel, Optimization of codon translation rates via tRNA modifications maintains proteome integrity. *Cell* **161**, 1606–1618 (2015).

41. K. Sebastian *et al.*, Proteome organization in a genome-reduced bacterium. *Science* **326**, 1235–1240 (2009).
42. K. M. Wegener *et al.*, Global proteomics reveal an atypical strategy for carbon/nitrogen assimilation by a cyanobacterium under diverse environmental perturbations. *Mol. Cell. Proteomics* **9**, 2678–2689 (2010).
43. S. Duret *et al.*, Invasion of insect cells by *Spiroplasma citri* involves spiralin relocalization and lectin/glycoconjugate-type interactions. *Cell. Microbiol.* **16**, 1119–1132 (2014).
44. T. Pascucci, J. Perrino, A. P. Mahowald, G. L. Waring, Eggshell assembly in *Drosophila*: Processing and localization of vitelline membrane and chorion proteins. *Dev. Biol.* **177**, 590–598 (1996).
45. H. Li *et al.*, Fly cell atlas: A single-cell transcriptomic atlas of the adult fruit fly. bioRxiv (2021). DOI: 10.1126/science.abk2432.
46. J. K. Herren, B. Lemaitre, *Spiroplasma* and host immunity: Activation of humoral immune responses increases endosymbiont load and susceptibility to certain Gram-negative bacterial pathogens in *Drosophila melanogaster*. *Cell. Microbiol.* **13**, 1385–1396 (2011).
47. M. Liu *et al.*, Tango1 spatially organizes ER exit sites to control ER export. *J. Cell Biol.* **216**, 1035–1049 (2017).
48. C. Pfeiffenberger, B. C. Lear, K. P. Keegan, R. Allada, Locomotor activity level monitoring using the *Drosophila* activity monitoring (DAM) system. *Cold Spring Harbor Protoc.* **2010**, pdb.prot5518 (2010).
49. F. Masson, F. Schüpfer, C. Jollivet, B. Lemaitre, Transformation of the *Drosophila* sex-manipulative endosymbiont *Spiroplasma poulsonii* and persisting hurdles for functional genetic studies. *Appl. Environ. Microbiol.* **86**, e00835-20 (2020).
50. Y. Romeo, B. Lemaitre, "Drosophila immunity, methods for monitoring the activity of toll and imd signaling pathways" in *Innate Immunity*, J. Ewbank, E. Vivier, Eds. (Humana Press, 2008), pp. 379–394.
51. M. W. Pfaffl, A new mathematical model for relative quantification in real-time RT-PCR. *Nucleic Acids Res.* **29**, e45 (2001).
52. J. Rappsilber, M. Mann, Y. Ishihama, Protocol for micro-purification, enrichment, pre-fractionation and storage of peptides for proteomics using StageTips. *Nat. Protoc.* **2**, 1896–1906 (2007).
53. J. Cox, M. Mann, MaxQuant enables high peptide identification rates, individualized p.p.b.-range mass accuracies and proteome-wide protein quantification. *Nat. Biotechnol.* **26**, 1367–1372 (2008).
54. J. Cox *et al.*, Accurate proteome-wide label-free quantification by delayed normalization and maximal peptide ratio extraction, termed MaxLFQ. *Mol. Cell. Proteomics* **13**, 2513–2526 (2014).
55. S. Tyanova *et al.*, The Perseus computational platform for comprehensive analysis of (prote)omics data. *Nat. Methods* **13**, 731–740 (2016).